






## Pathogenic *WDFY3* variants cause neurodevelopmental disorders and opposing effects on brain size

 Diana Le Duc,<sup>1</sup> Cecilia Giulivi,<sup>2,3</sup> Susan M. Hiatt,<sup>4</sup> Eleonora Napoli,<sup>2</sup>  
 Alexios Panoutsopoulos,<sup>5,6</sup>  Angelo Harlan De Crescenzo,<sup>5,6</sup> Urania Kotzaeridou,<sup>7</sup>  
 Steffen Syrbe,<sup>7</sup> Evdokia Anagnostou,<sup>8</sup> Meron Azage,<sup>9</sup> Renee Bend,<sup>10</sup> Amber Begtrup,<sup>11</sup>  
 Natasha J. Brown,<sup>12,13,14</sup> Benjamin Büttner,<sup>1</sup> Megan T. Cho,<sup>11</sup> Gregory M. Cooper,<sup>4</sup>  
 Jan H. Doering,<sup>7</sup> Christèle Dubourg,<sup>15,16</sup> David B. Everman,<sup>10</sup> Michael S. Hildebrand,<sup>12,17</sup>  
 Francis Jeshira Reynoso Santos,<sup>18</sup> Barbara Kellam,<sup>19</sup> Jennifer Keller-Ramey,<sup>11</sup>  
 Johannes R. Lemke,<sup>1</sup> Shuxi Liu,<sup>11</sup> Dmitriy Niyazov,<sup>9</sup> Katelyn Payne,<sup>20</sup> Richard Person,<sup>11</sup>  
 Chloé Quélin,<sup>21</sup> Rhonda E. Schnur,<sup>11</sup> Brooke T. Smith,<sup>10</sup> Jonathan Strober,<sup>22</sup> Susan Walker,<sup>19</sup>  
 Mathew Wallis,<sup>23,24</sup> Laurence Walsh,<sup>20</sup> Sandra Yang,<sup>11</sup> Ryan K.C. Yuen,<sup>19,25</sup>  
 Andreas Ziegler,<sup>7</sup> Heinrich Sticht,<sup>26</sup> Michael C. Pride,<sup>3,27</sup> Lori Orosco,<sup>5,6</sup>  
 Verónica Martínez-Cerdeño,<sup>3,5,6</sup> Jill L. Silverman,<sup>3,27</sup> Jacqueline N. Crawley,<sup>3,27</sup>  
 Stephen W. Scherer,<sup>19,28</sup> Konstantinos S. Zarbalis<sup>3,5,6</sup> and Rami Jamra<sup>1</sup>

The underpinnings of mild to moderate neurodevelopmental delay remain elusive, often leading to late diagnosis and interventions. Here, we present data on exome and genome sequencing as well as array analysis of 13 individuals that point to pathogenic, heterozygous, mostly *de novo* variants in *WDFY3* (significant *de novo* enrichment  $P = 0.003$ ) as a monogenic cause of mild and non-specific neurodevelopmental delay. Nine variants were protein-truncating and four missense. Overlapping symptoms included neurodevelopmental delay, intellectual disability, macrocephaly, and psychiatric disorders (autism spectrum disorders/attention deficit hyperactivity disorder). One proband presented with an opposing phenotype of microcephaly and the only missense-variant located in the PH-domain of *WDFY3*. Findings of this case are supported by previously published data, demonstrating that pathogenic PH-domain variants can lead to microcephaly via canonical Wnt-pathway upregulation. In a separate study, we reported that the autophagy scaffolding protein *WDFY3* is required for cerebral cortical size regulation in mice, by controlling proper division of neural progenitors. Here, we show that proliferating cortical neural progenitors of human embryonic brains highly express *WDFY3*, further supporting a role for this molecule in the regulation of prenatal neurogenesis. We present data on Wnt-pathway dysregulation in *Wdfy3*-haploinsufficient mice, which display macrocephaly and deficits in motor coordination and associative learning, recapitulating the human phenotype. Consequently, we propose that in humans *WDFY3* loss-of-function variants lead to macrocephaly via downregulation of the Wnt pathway. In summary, we present *WDFY3* as a novel gene linked to mild to moderate neurodevelopmental delay and intellectual disability and conclude that variants putatively causing haploinsufficiency lead to macrocephaly, while an opposing pathomechanism due to variants in the PH-domain of *WDFY3* leads to microcephaly.

1 Institute of Human Genetics, University Medical Center Leipzig, Leipzig, 04103, Germany

2 Department of Molecular Biosciences, School of Veterinary Medicine, University of California Davis, Davis, CA 95616, USA

3 MIND Institute, University of California Davis, Sacramento, CA 95817, USA

- 4 HudsonAlpha Institute for Biotechnology, 601 Genome Way, Huntsville, AL 35806, USA
- 5 Department of Pathology and Laboratory Medicine, University of California at Davis, Sacramento, CA 95817, USA
- 6 Institute for Pediatric Regenerative Medicine, Shriners Hospitals for Children, Sacramento, CA 95817, USA
- 7 Division of Child Neurology and Inherited Metabolic Diseases, Centre for Paediatrics and Adolescent Medicine, University Hospital Heidelberg, Im Neuenheimer Feld 430, Heidelberg, 69120, Germany
- 8 Bloorview Research Institute, University of Toronto, Toronto, M4G 1R8, Canada
- 9 Department of Pediatrics, Ochsner Health System and University of Queensland, New Orleans, LA 70121, USA
- 10 Greenwood Genetic Center, Greenwood, SC 29646, USA
- 11 GeneDx, Clinical Genomics, 207 Perry Parkway Gaithersburg, MD 20877, USA
- 12 Department of Pediatrics, University of Melbourne, VIC 3010, Australia
- 13 Victorian Clinical Genetics Services, Parkville, VIC 3052, Australia
- 14 Murdoch Children's Research Institute, Parkville, VIC 3052, Australia
- 15 Service de Génétique Moléculaire et Génomique, CHU, Rennes, F-35033, France
- 16 Univ Rennes, CNRS, IGDR, UMR 6290, Rennes, F-35000, France
- 17 Epilepsy Research Centre, Austin Health, Heidelberg, VIC 3010, Australia
- 18 Joe DiMaggio Children's Hospital, Hollywood, FL 33021, USA
- 19 The Centre for Applied Genomics, The Hospital for Sick Children, Toronto, M5G 0A4, Canada
- 20 Riley Hospital for Children, Indianapolis, IN 46202, USA
- 21 Service de Génétique Clinique, CHU, Rennes, F-35203, France
- 22 UCSF Benioff Children's Hospital, San Francisco, CA 94158, USA
- 23 Austin Health Clinical Genetics Service, Heidelberg, VIC 3084, Australia
- 24 Department of Medicine, University of Melbourne, Parkville, VIC 3010, Australia
- 25 Department of Molecular Genetics, University of Toronto, Toronto, ON M5S 1A8, Canada
- 26 Institute of Biochemistry, Emil-Fischer-Center, Friedrich-Alexander-Universität Erlangen-Nürnberg, Erlangen, 91054, Germany
- 27 Department of Psychiatry and Behavioral Sciences, University of California Davis, Davis, CA 95616, USA
- 28 McLaughlin Centre, University of Toronto, Toronto, ON M5G 0A4, Canada

Correspondence to: Rami Jamra, MD  
 Institute of Human Genetics, University Medical Center Leipzig, Philipp-Rosenthal-Str. 55,  
 04103 Leipzig, Germany  
 E-mail: rami.aboujamra@medizin.uni-leipzig.de

Correspondence may also be addressed to: Konstantinos Zarbalis, PhD  
 Institute for Pediatric Regenerative Medicine, Shriners Hospitals for Children, Northern  
 California, Sacramento, CA 95817, USA  
 E-mail: kzarbalis@ucdavis.edu

**Keywords:** *WDFY3*; brain size; neurodevelopmental delay; intellectual disability

## Introduction

Neurodevelopmental delay is a heterogeneous disorder that can be classified as mild if the functional age is above 67% of the development corresponding to the chronological age, or moderate if functional age is 34–66% of chronological age (McDonald *et al.*, 2006). While next-generation sequencing has proven successful in understanding the genetic causes of severe forms of neurodevelopmental delay and associated intellectual disability, the genetic basis of mild to moderate neurodevelopmental delay has yet to be satisfactorily explained (Vissers *et al.*, 2016).

Here we describe how the advent of next-generation sequencing corroborated with international collaboration (Sobreira *et al.*, 2015) can facilitate the discovery of monogenic causes for mild to moderate neurodevelopmental delay and end a diagnostic odyssey. We report on 13 probands with mild to moderate neurodevelopmental delay and intellectual disability caused by heterozygous variants in *WDFY3*.

*WDFY3* has been already reported as relevant for higher cognitive functions through its association with autism spectrum disorders (Iossifov *et al.*, 2012, 2014; Wang *et al.*, 2016; Stessman *et al.*, 2017; Yuen *et al.*, 2017) (SFARI gene category 2.1). Also, a missense variant, located in the PH-domain of *WDFY3*, has been linked to moderate intellectual disability and microcephaly in a large kindred, through modification of *Dvl3* autophagy-mediated control of the canonical Wnt signalling pathway (Kadir *et al.*, 2016).

*WDFY3* encodes for autophagy-linked FYVE protein (also named ALFY), a large multidomain scaffolding protein implicated in the selective degradation of ubiquitinated protein aggregates by autophagy (Filimonenko *et al.*, 2010) and clearance of mitochondria via mitophagy (Napoli *et al.*, 2018). In mice, *Wdfy3* is expressed in the neocortex of the developing embryo, where we have previously shown that it regulates the proliferation of neural progenitors with loss-of-function leading to an expansion of the radial glial cell population (Orosco *et al.*, 2014).

In this study, we describe the impact of deleterious *WDFY3* heterozygous variants on human neurodevelopment and provide a detailed clinical description of identified cases. We also show that the human macrocephaly phenotype is recapitulated in a *Wdfy3*-haploinsufficiency mouse model. Using proteomics analysis we investigated the effect of *Wdfy3*-haploinsufficiency on Wnt-pathway signalling and show different outputs based on different putative pathomechanisms.

## Material and methods

### Ethics approval

This study was approved and monitored by the ethics committee of the University of Leipzig, Germany (224/16-ek and 402/16-ek), the review boards at Western (20130675), and the University of Alabama at Birmingham (X130201001). Institutional ethics approval was not required if testing was part of routine clinical care. All families provided informed consent for clinical testing and publication.

### Sequencing

Probands were tested mainly in trio-exome or -genome sequencing setup (Supplementary material), with the exception of Proband 13, whose deletion was identified by single nucleotide polymorphism microarray. Bioinformatic processing and evaluation of identified and annotated variants were performed at different centres using either in-house pipelines or commercial software. The evaluation of the cases was first performed in a diagnostic setting, which revealed no causative variant. Downstream analysis of genes not yet related to neurodevelopmental disorders revealed *WDFY3* as the sole convincing candidate gene. All variants in *WDFY3* that were not detected by sequencing a parent-child trio or where the quality of the massive parallel sequencing was insufficient were confirmed by Sanger sequencing. Further details on sequencing methods can be obtained from previous publications of the different centres (Bowling *et al.*, 2017; Martin *et al.*, 2017; Retterer *et al.*, 2016; Yuen *et al.*, 2017). A detailed description of the sequencing setup is provided in the Supplementary material.

### Molecular modelling

The PH-BEACH domain pair of *WDFY3* was modelled using the crystal structure of the homologous domain pair from human LRBA/BGL (PDB: 1T77; Gebauer *et al.*, 2004) as a template. HHpred (Zimmermann *et al.*, 2018) was used for sequence alignment and Modeller (Webb and Sali, 2017) for modelling. The model comprises residues 2534–2976 of *WDFY3*, with the exception of the sequence stretch 2582–2599 that exhibits no homology to the

template structure. Mutations were modelled with SwissModel (Guex and Peitsch, 1997) and RasMol (Sayle and Milner-White, 1995) was used for structure analysis and visualization.

### WDFY3 embryonic expression analysis

Immunostaining was carried out on slide-mounted 6- $\mu$ m thick fixed sections of human forebrain. Human foetal tissue was donated by the next of kin to the Program of Body Donation for Teaching and Research at the Universidad Autónoma de Madrid School of Medicine. In brief, tissue was washed prior to antigen retrieval and after antigen retrieval the tissue was also repeatedly rinsed.  $\alpha$ -*Wdfy3* (Abnova) and secondary antibody (Biotin-SP-APure F(ab')<sub>2</sub> Frag Dnk Anti-Mse IgG (H+L), Jackson ImmunoResearch) were applied consequently. Then, we incubated the tissue with Avidin-Biotin (AB) Complex (Vector Laboratories) and visualized the signal using 3,3'-diaminobenzidine tetrahydrochloride (Sigma). A detailed description of antibody incubation is provided in the Supplementary material. After labelling procedures, tissue sections were post-fixed, dehydrated, mounted, and photomicrographs were taken on an Olympus BX61 microscope at  $\times 10$  and  $\times 100$  magnification.

### Animal husbandry and behavioural tests

Generation and genotyping of *Wdfy3<sup>+lacZ</sup>* mice was described elsewhere (Orosco *et al.*, 2014). Animals tested were of either sex.

We tested the motor skill performance of 2–3-month-old mice on a rotarod apparatus (Rota-rod/RS, PanLab Harvard Apparatus). Trials were recorded using the SeDaCom software system (version 1.4.02, PanLab Harvard Apparatus).

Contextual and cued fear conditioning was used to evaluate memory of an aversive experience associated with the stimuli present during the aversive event. On Day 1, we placed 3–4-month-old mice in a metal chamber with a grid floor and allowed them to explore for 2 min. An auditory stimulus was presented for 30 s during the last second of which a 2-s 0.5 mA AC current foot-shock was delivered. On Day 2, mice were returned to the same testing chamber without foot-shock administration and we tested whether they remembered the association of foot-shock with contextual features of the chamber by measuring freezing time. On Day 3, we placed the mice in a different testing chamber (curved shape, Plexiglas floor surfaces, white light, and vanilla extract odour). Freezing in the new context was minimal since no aversive experience had occurred in the new context. Then we played the auditory stimulus for 3 min with no foot-shock and we scored freezing as the measure of cued fear conditioning. A

detailed description of the behavioural tests setup is provided in the Supplementary material.

## Wnt proteomics of cortical lysates of *Wdfy3* haploinsufficient mice

### Sample preparation

We used cortices from seven wild-type and seven *Wdfy3*<sup>+/*lacZ*</sup> 3-month-old female mice to obtain protein-enriched fractions as described previously (Napoli *et al.*, 2018). Proteins were evaluated using the Pierce BCA protein assay (Thermo Scientific).

### Mass spectrometry

Liquid chromatography (LC) with tandem mass spectrometry (MS) was performed at the University of California Davis Genome Center Core Proteomics Facility. Protein pellets were digested overnight with a trypsin to protein ratio of 1:30. For each sample, the equivalent of 2–5 µg of protein was loaded into the LC-MS/MS.

### Database searching

All LC/MS samples were analysed using X! Tandem [The GPM, thegpm.org; version TORNADO (2010.01.01.4)]. X! Tandem was set up to search the uniprot\_20120523\_gTmkm3 database (89 576 entries) assuming trypsin digestion. X! Tandem was searched with a fragment ion mass tolerance of 20 ppm and a parent ion tolerance of 1.8 Da. Deamidation of Asn and Gln, oxidation of Met and Trp, sulphonation of Met, Trp oxidation to formylkynurenin, and acetylation of the N-terminus were specified in X! Tandem as variable modifications.

### Criteria for protein identification

Scaffold (v. 3.00.07, Proteome Software Inc., Portland, OR) was used to validate LC/MS based peptide and protein identification. Peptide identification was accepted if it could be established at >80% probability by the Peptide Prophet algorithm (Keller *et al.*, 2002). Protein identifications were accepted if they could be established at >80% probability and contained at least two identified peptides. Protein probabilities were assigned by the Protein Prophet algorithm (Nesvizhskii *et al.*, 2003). Proteins that contained similar peptides and could not be differentiated based on LC/MS analysis alone were grouped to satisfy the principles of parsimony.

### Proteomics analysis

The proteome profiles from all 14 animals were normalized by their spectral counting sum. We used partial least squares discriminant analysis to identify the features that separated the two genotypes the most. The proteins that best described the differences between the two groups were selected by setting a variable in importance projection score of >0.8.

## Statistical analysis

To test whether there is a significant enrichment of *WDFY3 de novo* variants in a neurodevelopmental delay cohort compared to the occurrence by chance, we used a binomial test in R (Core, 2017). Further, we used a Bonferroni correction to adjust the *P*-value for multiple testing considering 18 894 coding sequences according to the latest release of the consensus coding sequence (CCDS) project (Pruitt *et al.*, 2009) (v.20 interrogated in May 2018).

For the proteomics analyses, proteins associated with the gene ontology term ‘Wnt’ (under biological process) and a *P*-value corrected by the FDR (false discovery rate) of ≤0.10 were considered to have a significant differential expression.

To test the enrichment of probands with occipital-frontal circumference (OFC) over the 87th percentile compared to the OFC distribution in normal population we used a binomial test function (Core, 2017). All other statistics related to *Wdfy3*<sup>+/*lacZ*</sup> were performed with unpaired *t*-tests and bars represent mean ± standard error of the mean (SEM). The difference between groups was considered statistically significant at *P*-value < 0.05.

## Data availability

The data that support the findings of this study are available from the corresponding author, upon reasonable request.

## Results

### Phenotypic characterization of probands

Thirteen probands (2–18 years old) were clinically examined at several centres in North America, Europe, and Australia. All individuals were reported to have cognitive and/or developmental deficits. Mild to moderate intellectual disability (defined as mild intellectual disability if the functional age was above 67% of the corresponding chronological age development or moderate if the functional age corresponded to 34–66% of chronological age) was observed in 8/10 (80%) cases for whom intellectual assessment was performed (Fig. 1A and Table 1). Information on quantitative diagnostic standardization was not obtainable, because testing was performed in multiple clinical centres that are, however, specialized in developmental delay. Delayed speech was common in examined individuals (11/13, 85%), as was gross motor development delay or muscular hypotonia (7/13, 54%; Fig. 1A and Table 1). Behavioural concerns were noted in 9/12 assessed individuals (75%) including autism spectrum disorder (7/12) and attention deficit hyperactivity disorder (4/12) (Fig. 1A and Table 1). There was no apparent shared facial gestalt. Macrocephaly or large-normal OFC was observed in 9/11



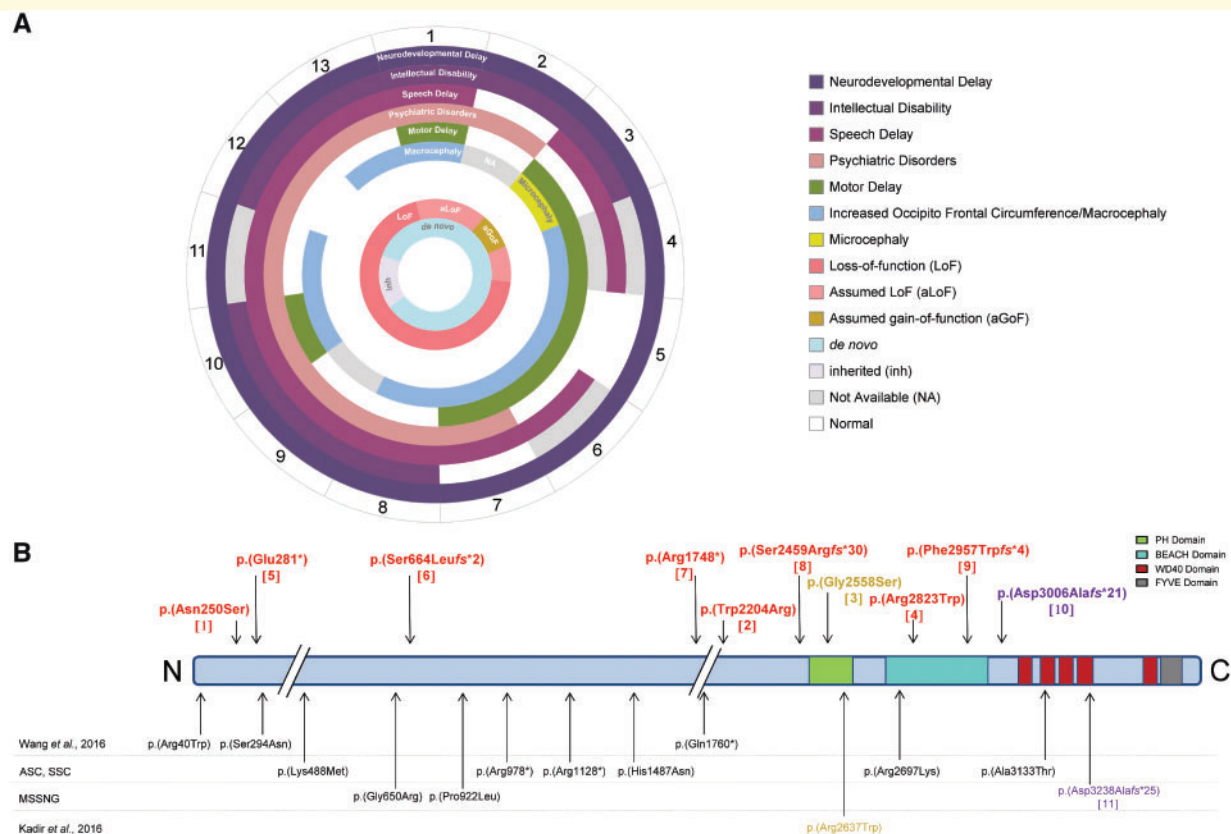


**Figure 1 Summary of genotypes and phenotypes of individuals with WDFY3-related neurodevelopmental delay. (A)** Outer circle: proband number (Table 1). Second to seventh circles: clinical symptoms, phenotype. Inner circles: genotype. **(B)** *De novo* missense, nonsense, and frameshift variants (NM\_014991.4) from patients with neurodevelopmental delay and macrocephaly described in the present study (red, proband number in square brackets; Table 1). *De novo* variants described in previous autism spectrum disorder cohorts [bottom: black; Autism Speaks MSSNG, Autism Sequencing Consortium (ASC) and Simons Simplex Collection (SSC)] (Wang *et al.*, 2016; Yuen *et al.*, 2017). Variants in yellow occurred in probands with neurodevelopmental delay and microcephaly (*upper panel* variant occurred *de novo*, *lower panel* variant previously described in a kindred (Kadir *et al.*, 2016)). Variants depicted in purple are inherited from an affected father, otherwise all presented variants occurred *de novo*.

evaluated cases (5/9 >97th percentile and 4/9 between 87th and 95th percentiles) (Fig. 1A and Table 1). Statistical analysis revealed an enrichment of probands with OFC over the 87th percentile in our cohort compared to the distribution in general population ( $P = 4.548 \times 10^{-7}$ ). We did not observe any differences in the phenotypical spectrum of probands bearing missense variants located outside organized protein domains (Proband 1 and 2; Fig. 1 and Table 1) or in the BEACH-Domain (Proband 4; Fig. 1 and Table 1) compared to probands bearing truncating variants (Proband 5–12; Fig. 1 and Table 1). However, the proband with a *de novo* variant located in the PH-domain (Proband 3; Fig. 1 and Table 1) displayed overt microcephaly [OFC = 42 cm, under the 3rd centile;  $-8.78$  standard deviation (SD)]. This patient was also diagnosed with cystic fibrosis and showed typical signs of dystrophy related to the condition [short stature: 92 cm, under the 3rd centile,  $-3.95$  SD; low weight 10.86 kg, under the 3rd centile,  $-4.72$  SD; body mass index (BMI) 12.8 kg/m<sup>2</sup>, under the

3rd centile,  $-2.02$  SD]. Nonetheless, microcephaly is not associated with cystic fibrosis. Brain MRI was available on nine individuals, of whom six were reported as normal or unremarkable, and abnormal in the remaining three without specific or overlapping features. Detailed clinical information is described in the Supplementary material, Case reports are summarized in Fig. 1 and Table 1.

## Identified variants and their characteristics

We identified heterozygous *de novo* missense-variants in WDFY3 (MIM: 617485, NM\_014991.4) in four probands: c.749A > G: p.(Asn250Ser), c.6610T > C: p.(Trp2204Arg), c.7672G > A: p.(Gly2558Ser), and c.8467C > T: p.(Arg2823Trp). Five probands had *de novo* truncating-variants: c.841G > T: p.(Glu281\*), c.1990delT: p.(Ser664Leufs\*2), c.5242C > T: p.(Arg1748\*), c.7372\_7373insGA: p.(Ser2459Argfs\*30), and c.8867\_8868insTTGG: p.(Phe

**Table 1** Main clinical features of the probands

Patient identifier	1	2	3	4	5	6	7
<b>Genotype</b>	85752586T>C	85658484A>G	85639657C>T	85623635G>A	85750272C>A	85731395del	85678261G>A
Genomic position chr4	c.749A>G	c.6610T>C	c.7672G>A	c.8467C>T	c.841G>T	c.1990delT	c.5242C>T
Protein alteration	p.(Asn250Ser)	p.(Trp2204Arg)	p.(Gly2558Ser)	p.(Arg2823Trp)	p.(Glu281*)	p.(Ser664Leufs*2)	p.(Arg1748*)
Zygosity	Het	Het	Het	Het	Het	Het	Het
Inheritance	De novo	De novo	De novo	De novo	De novo	De novo	De novo
<b>Patient details</b>							
Age of patient, sex	14 y, M	15y, F	5 y, F	2 y, M	4 y, M	5 y, M	4 y, M
OFC	57.7 cm (P87th)	Not available	42 cm (<P3th; -8.78 SD)	52 cm (>P97th; +2.03 SD)	54.8 cm (>P97th; +2.88 SD)	55.5 cm (>P97th; +3.01 SD)	52 cm (P90th)
Height	168 cm (P67th)	163.5 cm (P41th)	92 cm (<P3rd; -3.95 SD)	84 cm (P12th)	88.3 cm (<P3rd; -3.61 SD)	114.8 cm (P89th)	95 cm (<P3rd; -2.08 SD)
Weight	59.8 kg (P74th)	65.4 kg (P83th)	10.86 kg (<P3th; -4.72 SD)	9.5 kg (P2th; -2.12 SD)	14.3 kg (P25th)	20.1 kg (P74th)	14.4 kg (P10th)
<b>Neurodevelopment</b>							
Neurodevelopmental delay	Yes	Yes	Yes	Yes	Yes	Yes	Yes
Intellectual disability	Mild ID	Mild ID	Moderate ID	Not available	Normal	Not available	Normal
Speech and language	Speech delay, stutter	Speech delay, stutter	Speech delay (a few words, no word association)	Speech delay	Normal	Speech delay; first words after 2y	Speech delay
Motor development	Gross motor delay, mild truncal hypotonia, abnormal gait	Gross motor delay, ADHD	Gross motor delay (walk at 2 y)	Gross motor delay at 2 y	Gross motor delay, truncal hypotonia, improved, intoeing	Gross motor delay	Motor delay, muscular hypotonia
Behavioural issues	ADHD	ADHD, anxiety, depression	None	Not available	None	None	Suspected ASD
<b>Patient identifier</b>	<b>8</b>	<b>9</b>	<b>10</b>	<b>11<sup>a</sup></b>	<b>12<sup>a</sup></b>	<b>13</b>	
<b>Genotype</b>	85645644_85645645dup	85617157_85617160dup	85614060_85614070del	85605108_85605111del	85605095del	4q21.23del: 85,665,448-86,686,764del	
Genomic position chr4	c.7371_7372insGA	c.8867_8868insTTGG	c.9017_9027del	c.9711_9714del	c.9726+1del	c.?	
cDNA (NM_014991.4)	p.(Ser2459Arg)*30	p.(Phe2957Trp)*4	p.(Asp3006Ala)*21	p.(Asp3238Glu)*25	p.?	p.?	
Protein alteration	Het	Het	Het	Het	Het	Het	
Zygosity	De novo	De novo	Paternally inherited	Paternally inherited	De novo	De novo	
Inheritance							
<b>Patient details</b>							
Age of patient, sex	2 y 9m, M	7 y, F	17 y, M	ca. 12 y, M	10 y 2 m, F	11 y 9 m, M	
OFC	53.8 cm (>P97th; +2.67 SD)	Not available	59 cm (P94th)	57.5 cm (>P97th; +2.18 SD)	50.8 cm (P6th)	56.5 cm (P95th)	
Height	95 cm (P50-75th)	132 cm (P93th)	181.5 cm (P75-90th)	153.7 cm (P59th)	127 cm (<P3rd; -2.22 SD)	153 cm (P76th)	
Weight	17.5 kg (P97th)	21.32 kg (P20th)	97.7 kg (>P97th, +3 SD)	50.8 kg (P82nd)	25.54 kg (P4th)	43.2 kg (P67th)	
<b>Neurodevelopment</b>							
Neurodevelopmental delay	Yes	Yes	Yes	Yes	Yes	Yes	
Intellectual disability	Mild ID	Moderate ID	Mild ID	Not available	Moderate ID	Mild ID	
Speech and language	Speech delay, single words at age of 2 y	Speech delay	Speech delay	Speech delay; below average based on Vineland scores	Speech delay	Speech delay	
Motor development	Normal	Normal	Motor delay, muscular hypotonia in early childhood	Normal	Normal	Normal	
Behavioural issues	ASD, easily frustrated	ASD	ASD	ASD, ADHD	ASD	ASD, ADHD	

ADHD = attention deficit hyperactivity disorder; ASD = autism spectrum disorder; F = female; Het = heterozygous; ID = intellectual disability, m = months; M = male; OFC = occipitofrontal circumference; P = percentile; y = years. <sup>a</sup>Patients from the Autism Speaks MSSNG cohort (Yuen et al., 2017).

2957Trpfs\*4). In one proband we identified a *de novo* splicing variant involving the conserved consensus splicing site c.9726+1del and affecting the donor site located on intron 64 and another proband had a *de novo* heterozygous 1.0 Mb deletion within 4q21.23 (chr4: g.85,665,448–86,686,764) including the first 36 exons of *WDFY3* and the first three exons of *ARHGAP24* (tolerates haploinsufficiency with a pLi score of 0). We also identified a familial variant of a 11-bp deletion, c.9017\_9027del: p.(Asp3006Alafs\*21), present in a proband and inherited from his similarly affected father, who presented with a moderate intellectual deficit (Supplementary material, Case reports, Proband 10). An additional paternally inherited variant, c.9711\_9714del: p.(Asp3238Glufs\*25, was identified in a child with mild intellectual deficit and macrocephaly (cognitive performance has not been assessed for the parents). None of these variants was present in public databases [gnomAD; accessed in September 2018 (Lek *et al.*, 2016) or 1000 Genomes (Genomes Project *et al.*, 2015)]. For the missense variants, most of the *in silico* tools predicted pathogenicity (Kumar *et al.*, 2009; Adzhubei *et al.*, 2010; Pollard *et al.*, 2010; Schwarz *et al.*, 2014). The scaled CADD scores of the missense variants (Supplementary Table 1) ranged between 21 (corresponding to the top 1% deleterious variants in the human genome) and 32 (top 0.1% deleterious variants in the human genome) (Rentzsch *et al.*, 2019). An overview of the genetic variants together with previously published variants of association studies in probands with autism spectrum disorder/neurodevelopmental delay is presented in Fig. 1B.

This patient series and the identified variants were collected through international collaboration with colleagues and data-sharing resources such as GeneMatcher (Sobreira *et al.*, 2015). The size of the tested cohorts at all contributing centres sums up to 11 743 probands with neurodevelopmental delay. We further added the MSSNG cohort [5205 whole genomes (Yuen *et al.*, 2017)] and the Chinese autism cohort from Wang *et al.* (2016) (4998 whole exomes, including Autism Sequencing Consortium and Simons Simplex Collection) that have previously reported *de novo* variants in *WDFY3* (Fig. 1B). These sum to 20 *de novo* variants in 21 946 individuals. The occurrence of *de novo* variants in these neurodevelopmental delay cohorts is significantly higher ( $P = 1.745 \times 10^{-7}$ ; corrected  $P$ -value = 0.003) than expected under the mutation rate of  $1.08997 \times 10^{-4}$  (missense, nonsense, and frameshift variants) estimated for *WDFY3* by Samocha *et al.* (2014).

Truncating variants may activate the mRNA surveillance nonsense-mediated decay, or if translated, may result in a non-functional protein or a dominant negative effect. Such a pathogenic effect is not always clear for missense variants. All four missense variants in this study were conserved and predicted as pathogenic by most interrogated *in silico* evaluation tools. However, of the four missense

variants, we were not able to model the structural effect of the variants p.(Asn250Ser) and p.(Trp2204Arg) and infer the impact on protein functionality since these were not located in a domain with a described function. Since *WDFY3* binds phospholipids (Simonsen *et al.*, 2004; Cullinane *et al.*, 2013), we also checked whether the loss of a positive charge as consequence of the p.(Arg2823Trp) or the p.(Arg2637Trp) exchange might additionally affect phospholipid binding of the PH-BEACH domain pair. p.(Arg2637Trp) is located in the PH segment close to the canonical phospholipid binding pocket found in homologous PH domains. However, because this pocket is partially blocked by the protein chain in *WDFY3*, phospholipid binding would require some conformational rearrangement. p.(Arg2823Trp) is located in the BEACH segment of the domain pair, for which no structural information about ligand binding sites is known. Thus, based on the structural data available, no final conclusion can be drawn, whether the variants observed in the PH-BEACH domain pair affect phospholipid binding in addition to disturbing the protein structure.

The variant p.(Gly2558Ser) located in a  $\beta$ -turn of the PH-domain could not be reliably modelled due to low local sequence similarity to the template structure. The modelling template (PDB:1T77) has a bulky threonine instead of glycine at the corresponding sequence position thus favouring a different loop conformation. Still, in the PH-domain we could model the effect of the previously reported variant p.(Arg2637Trp) (Kadir *et al.*, 2016) (Fig. 2C). The results suggest that Arg2637 forms electrostatic interactions with Asp2635, which are lost in the p.(Arg2637Trp) variant leading to steric clashes and domain destabilization. Further, we also modelled the effect of the variant p.(Arg2823Trp), located in the BEACH-domain. The residue Arg2823 forms a salt-bridge with Asp2819 that stabilizes a turn in the BEACH-domain (Fig. 2). This bridge is lost in the p.(Arg2823Trp) variant (Fig. 2B), which may result in BEACH domain destabilization.

## WDFY3 expression in human prenatal brain

To examine *WDFY3* expression during developmental neurogenesis in humans, we proceeded to analyse *WDFY3* expression in human forebrain sections of gestational Weeks 15 and 17. *WDFY3* immunostaining revealed widespread and overlapping expression in the pallium of both brains encompassing all layers, yet with distinct differences between layers (Fig. 3A–C). Importantly, as in the murine *Wdfy3* KO model (Orosco *et al.*, 2014), radial glial cell-containing ventricular zone showed the strongest expression with high levels in radial units of the cortical plate. Progressively lower *WDFY3* expression was observed in the outer subventricular zone, inner subventricular zone, and subplate/intermediate zone. *WDFY3*-expressing cells

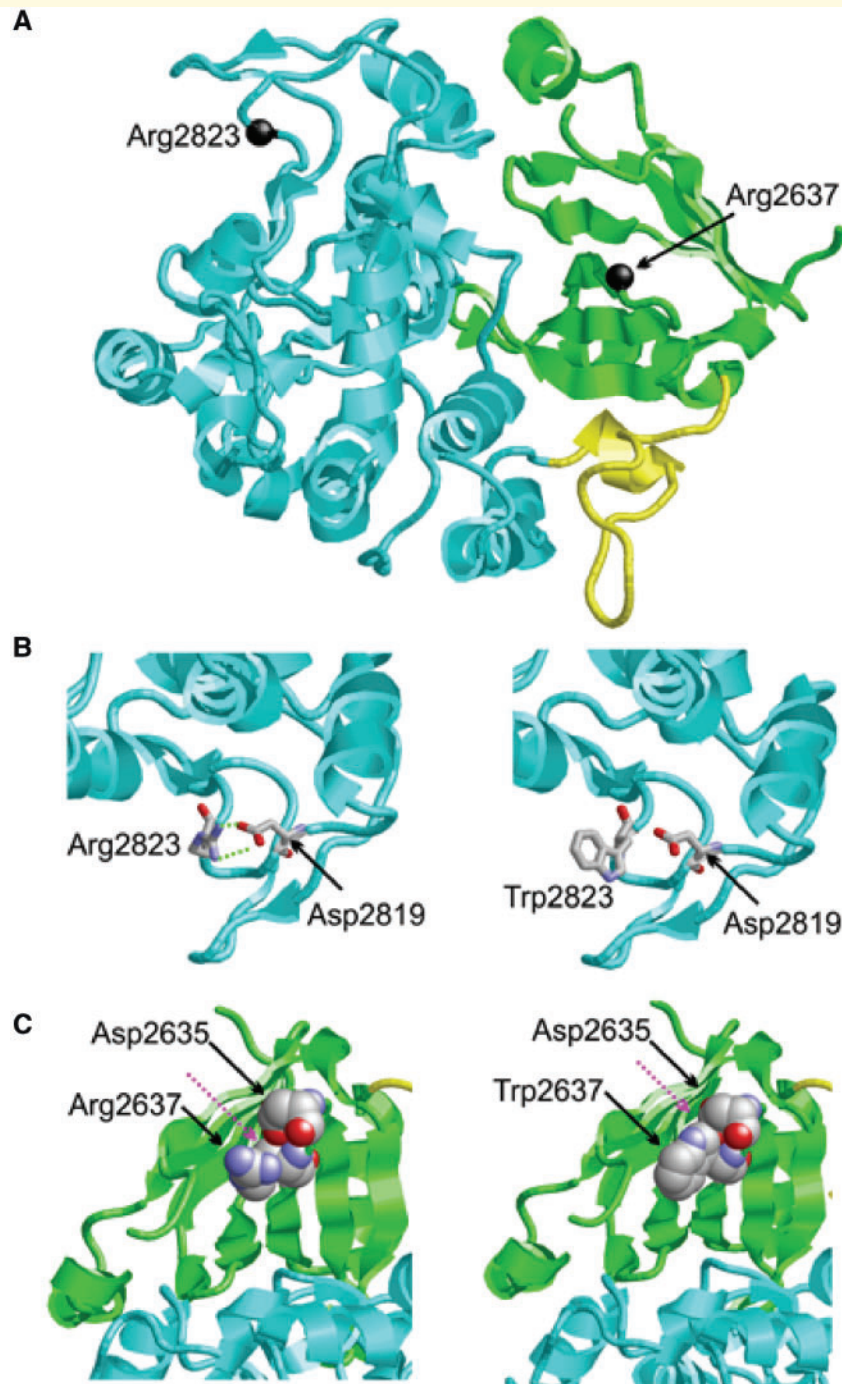


**Figure 2** Structural effects of WDFY3 sequence variants located in the BEACH- and PH-domains. **(A)** Modelled ribbon diagram of the wildtype domain pair of PH-domain (green) and BEACH-domain (cyan). The connecting linker is shown in yellow and the sites of the variants investigated are marked as black spheres. **(B)** Effect of the p.(Arg2823Trp) exchange in the BEACH-domain, associated in our study with neurodevelopmental delay and macrocephaly. Arg2823 forms a salt-bridge with Asp2819 (green dotted lines) that is lost in the Arg2823Trp variant. This likely leads to BEACH-domain destabilization. **(C)** Effect of the Arg2637Trp exchange, which has been associated with neurodevelopmental delay and microcephaly (Kadir *et al.*, 2016). Arg2637 forms electrostatic interactions with Asp2635, which are lost in the p.(Arg2637Trp) variant and steric clashes are observed instead. The magenta arrow marks the site of these opposing interactions. This likely leads to PH-domain destabilization.

do not show uniform expression levels, as they differ in signal intensity. Notably, dividing progenitors in the ventricular zone exhibit some of the strongest WDFY3

immunolabelling replicating aspects of WDFY3 expression previously observed in mice (Orosco *et al.*, 2014) (Fig. 3A–C).



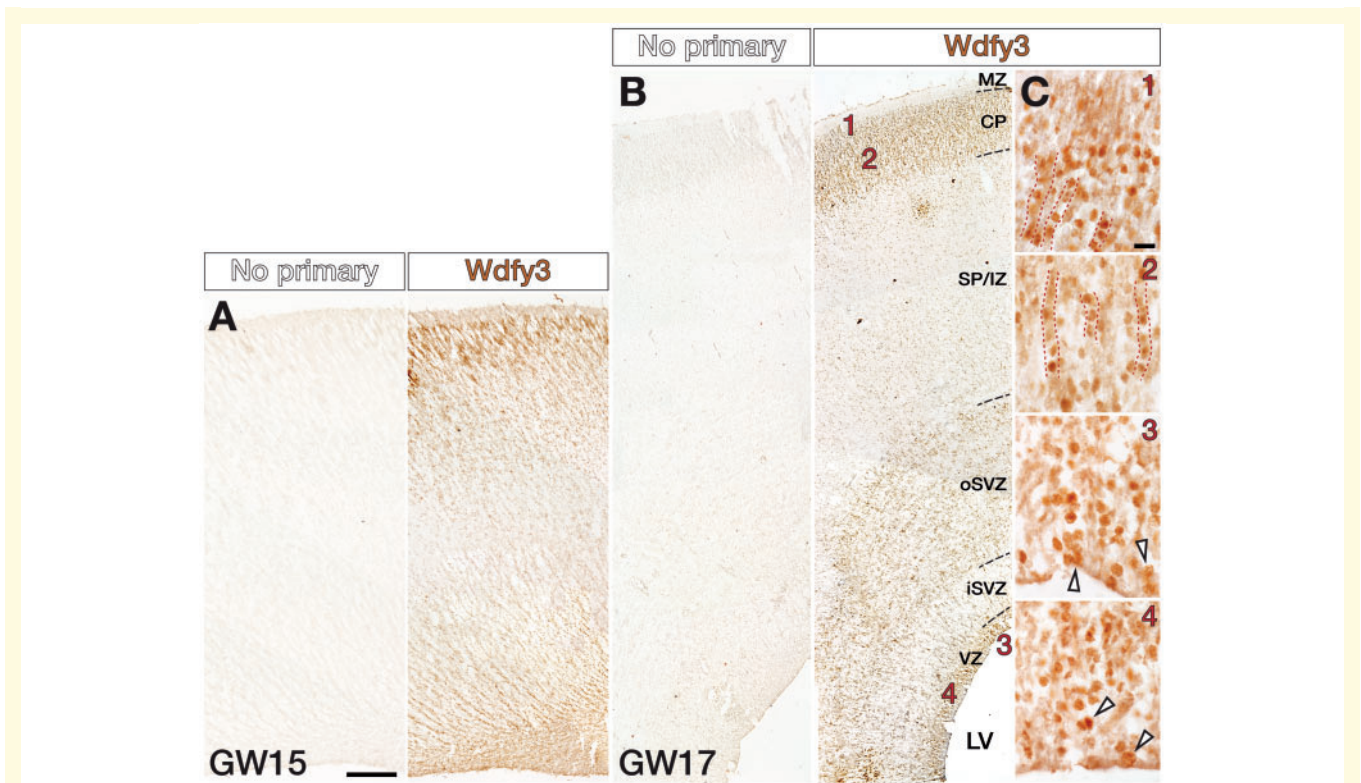


**Figure 3 WDFY3 expression in human embryonic pallium.** Sections of human ventral pallium reveal WDFY3 immunostaining at gestational Weeks (GW) 15 (**A**) and 17 (**B**). Pallial expression can be seen in all layers at varying degrees of intensity, with ventricular zone (VZ) and cortical plate (CP) containing the greatest proportion of WDFY3<sup>+</sup> cells. Lower WDFY3 expression is present in outer subventricular zone (oSVZ), inner subventricular zone (iSVZ), and subplate/intermediate zone (SP/IZ). Respective positions of high-magnification images in **C** are indicated as numbers in **B**. Some dividing progenitors in the ventricular zone exhibit strong WDFY3 immunolabelling (arrowheads) as some radial units of the cortical plate do (dotted lines). Scale bars = 500  $\mu$ m in **A** and **B**; 10  $\mu$ m in **C**.

### Macrocephaly in WDFY3 variant carriers and *Wdfy3*<sup>+/*lacZ*</sup> mice

As previously described in *Wdfy3* mouse models (Orosco *et al.*, 2014), probands with truncating variants had large head circumference (Fig. 1 and Table 1). While strongest cortical size increases were recorded in homozygous mouse mutants that are subject to perinatal lethality, heterozygous *Wdfy3*<sup>+/*lacZ*</sup> mice, which we analysed here further, survived into adulthood, were fertile, and presented at birth with structural abnormalities including cortical lengthening. Comparing whole-mount *Wdfy3*<sup>+/*lacZ*</sup> brains to wild-type controls at postnatal Days 7 and 10 revealed overt changes including significant cortical enlargement that apparently affected the anteroposterior axis to a greater extent than the medio-lateral axis (Fig. 4A). Cortical area enlargement was ~9% at postnatal Day 7 (wild-type, 0.753  $\pm$  0.01 cm<sup>2</sup>, *Wdfy3*<sup>+/*lacZ*</sup>, 0.824  $\pm$  0.01 cm<sup>2</sup>; Fig. 4B) and ~12% at postnatal Day 10 (wild-type, 1.095  $\pm$  0.03 cm<sup>2</sup>, *Wdfy3*<sup>+/*lacZ*</sup>, 1.229  $\pm$  0.02 cm<sup>2</sup>; Fig. 4C) without overt sex differences, mirroring the human large head circumference upon heterozygous WDFY3 loss.

### Motor coordination and associative learning deficits in *Wdfy3*<sup>+/*lacZ*</sup> mice

Multiple probands show gross motor abnormalities (Fig 1A and Table 1). Consequently, we tested motor coordination in *Wdfy3*<sup>+/*lacZ*</sup> mice by using the rotarod test. On three consecutive days, we compared the performance of *Wdfy3*<sup>+/*lacZ*</sup> to wild-type. *Wdfy3*<sup>+/*lacZ*</sup> mice ( $n = 6$ ) showed decreased endurance, learning, and motor coordination compared to wild-type mice ( $n = 8$ ), as the latency to fall off the rod was shorter for the *Wdfy3*<sup>+/*lacZ*</sup> mice in the acceleration test (4–40 rpm in 60 s; Fig. 4D).

Subsequently, we examined cognitive performance in *Wdfy3*<sup>+/*lacZ*</sup> mice, by testing associative learning with the contextual and cued fear conditioning test (Fanselow, 2000; LeDoux, 2003) in young males and nulliparous females. As shown in Fig. 4E, freezing to context on test Day 2 was significantly lower in the *Wdfy3*<sup>+/*lacZ*</sup> mice as compared to wild-type [Student's  $t(1,37) = 2.353$ ,  $P = 0.024$ ]. No differences between genotype groups were seen during the training Day 1, indicating normal perception and response to the foot-shock. No differences between

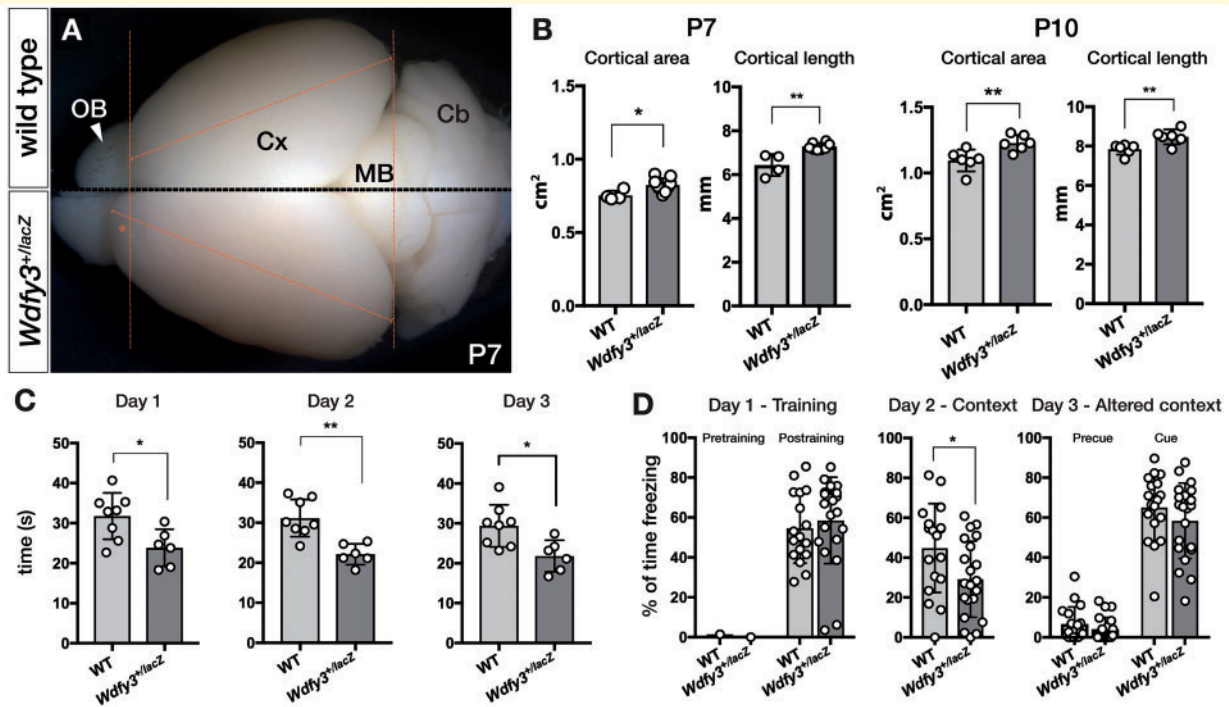


**Figure 4** *Wdfy3*<sup>+lacZ</sup> mice characteristics. Developmental megalecephaly in *Wdfy3*<sup>+lacZ</sup> mice. (A) Dorsal views of whole-mount PND7 brains show cerebral enlargement in *Wdfy3*<sup>+lacZ</sup> mice (indicated by the arrow; Cx = cortex, Cb = cerebellum, MB = midbrain). (B) For two postnatal stages [postnatal Day 7 (P7): wild-type *n* = 4, *Wdfy3*<sup>+lacZ</sup> *n* = 8 and postnatal Day 10 (P10): wild-type *n* = 6, *Wdfy3*<sup>+lacZ</sup> *n* = 6] both total cortical area (postnatal Day 7, *P* = 0.0273; postnatal Day 10, *P* = 0.0096) and cortical length (postnatal Day 7, *P* = 0.0012; postnatal Day 10, *P* = 0.008) were analysed and found to be significantly increased. Motor coordination and learning and memory deficits in *Wdfy3*<sup>+lacZ</sup> mice. (C) *Wdfy3*<sup>+lacZ</sup> mice show diminished motor coordination in the rotarod test [wild-type (WT) *n* = 8, *Wdfy3*<sup>+lacZ</sup> *n* = 6; Day 1, *t*(1,12) = 2.747, *P* = 0.0177; Day 2, *t*(1,12) = 4.258, *P* = 0.0011; Day 3, *t*(1,12) = 2.945, *P* = 0.0123]. (D) After footshock conditioning in the cued fear conditioning assay (Day 1), *Wdfy3*<sup>+lacZ</sup> mice exhibit learning and memory deficits in context freezing (Day 2), [*t*(1,37) = 2.353, *P* = 0.024], but not in cued freezing (Day 3) [*t*(1,37) = 1.158, *P* = 0.254]. All statistics were performed with unpaired *t*-tests and bars represent mean ± SEM.

*Wdfy3*<sup>+lacZ</sup> and wild-type mice were detected on auditory cue test Day 3, either during the pre-cue period or during the presentation of the auditory cue, indicating similar sensory, auditory skills (Fig. 4E).

Altogether, these results indicated that *Wdfy3*<sup>+lacZ</sup> mice ranging from 2 to 4 months of age showed impairment in motor coordination and the associative learning component of fear conditioned learning and memory.

## Wnt pathway analysis

Considering that Wnt signalling plays critical roles in normal brain development and neuropsychiatric disorders (Okerlund and Cheyette, 2011; Krumm et al., 2014; Hormozdiari et al., 2015; Kwan et al., 2016), and that *Drosophila* with a missense heterozygous variant p.(Arg263Trp) (Kadir et al., 2016) in the *WDFY3* homologue *Bchs* showed a lack of canonical Wnt signalling inhibition with its consequent uncontrolled upregulation, we performed an untargeted proteomic study on cortical neurons from 3-month-old wild-type and *Wdfy3*<sup>+lacZ</sup> females and focused our analysis on the entire Wnt pathway. We observed that *Wdfy3* haploinsufficiency was associated with a downregulation of the

degradation of beta-catenin by the destruction complex (FDR =  $1.45 \times 10^{-10}$ ) and by a relatively milder downregulation of both TCF-dependent signalling in response to Wnt (FDR =  $1.84 \times 10^{-14}$ ) and beta-catenin-independent Wnt-Ca<sup>2+</sup> signalling (FDR =  $1.84 \times 10^{-14}$ ; Supplementary Table 1 and Supplementary Fig. 1). The downregulation of the canonical Wnt pathway was supported mainly by the decreased levels of cytoplasmic b-catenin (*Ctmb1*; Tacchelly-Benites et al., 2013) as well as DVL1, CK2, GSK-3b, Pontin52. The lower levels of DVL1 seem to drive, albeit at a lower degree, the downregulation of the Wnt-dependent planar cell polarity (decreased levels of DVL1, Rac, and increased of RhoA) and Wnt/Ca<sup>2+</sup> pathways (decreased levels of CaN and increased of PLC and PKC; Supplementary Table 1 and Supplementary Fig. 2) based on the fact that Dvl proteins act at the node of divergence between the canonical and the non-canonical Wnt pathways (Gao and Chen, 2010). These results were extended by the upregulation of the proteasome pathway emphasizing the ubiquitin-mediated proteolytic catabolism of several key targets within the Wnt pathway, likely including Dvl (Supplementary Table 1 and Supplementary Fig. 2).

## Discussion

Our results show that pathogenic variants in *WDFY3* cause a monogenic, autosomal dominant neurodevelopmental disorder with mild to moderate neurodevelopmental delay and intellectual disability. Also, affected individuals showed deficits in motor coordination as well as behavioural disorders, with autism spectrum disorder as leading diagnosis. While putative haploinsufficiency of the gene leads to large head circumference, missense variants in the PH domain can cause the opposite phenotype—overt microcephaly.

Although data show that *WDFY3* is under constraint for missense variants (Z-score 5.72) (Lek *et al.*, 2016) and intolerant to loss of function [pLI = 1.00 (Lek *et al.*, 2016), RVIS = 0.1564% (Petrovski *et al.*, 2013)], there are 25 individuals with loss of function variants in the Genome Aggregation Database (gnomAD). Since *WDFY3* loss of function variants are mainly associated with mild developmental disorders, it is possible that such individuals are included in control cohorts. This is also supported by a recent study, which showed that 2.8% of the ExAC population (consequently also the overlapping gnomAD cohort) bears possible disease-associated genotypes, mainly for phenotypes with variable clinical outcomes or those that occur as mild forms of the disease (Tarailo-Graovac *et al.*, 2017). The number of identified *de novo* *WDFY3* variants in our combined cohort of probands with neurodevelopmental delay is significantly higher than the expected occurrence by chance, even after stringent multiple-testing correction ( $P = 0.003$ ).

Intolerance to loss of function is also supported by homozygous *Wdfy3* knock-out mouse models, which show perinatal lethality (Orosco *et al.*, 2014). We now show that heterozygous *Wdfy3<sup>+lacZ</sup>* mice survive into adulthood and are megalencephalic at young age (Fig. 3D–F), recapitulating the observation in the probands (Fig. 1A and Table 1). The molecular underpinnings of *WDFY3*'s essential role in brain size regulation were previously tested in *Drosophila* for a heterozygous missense variant p.(Arg2637Trp), which segregated in a large kindred with an autosomal dominant phenotype of microcephaly and moderate intellectual disability (Kadir *et al.*, 2016). This study concluded that the underlying molecular mechanism was based on a lack of canonical Wnt signalling inhibition with its consequent uncontrolled upregulation. Conversely, *Wdfy3<sup>+lacZ</sup>* mice show megalencephaly with a downregulation of the canonical Wnt pathway supported by our proteomic data (Supplementary Table 1 and Supplementary Fig. 1). Wnt proteins are required for basic developmental processes (e.g. cell-fate specification, progenitor-cell proliferation, and control of asymmetric cell division), and Wnt signalling plays critical roles in brain development and neuropsychiatric disorders (Okerlund and Cheyette, 2011), including autism spectrum disorders (Krumm *et al.*, 2014; Hormozdiari *et al.*, 2015; Kwan *et al.*, 2016). Our proteomic studies on cortical

lysates of haploinsufficient mice showed a downregulation of the canonical Wnt pathway and a relatively milder downregulation of the Wnt-dependent planar cell polarity pathway and Wnt/Ca<sup>2+</sup> pathways (Supplementary Table 1, Supplementary Figs 1 and 2). While the exact sequence of events leading to macrocephaly in humans and mice upon *WDFY3* loss remain uncertain, the downregulation of the canonical Wnt pathway will likely lead to cell cycle acceleration increasing proliferative and neurogenic rates of neural progenitors, a phenomenon that we had earlier described in *Wdfy3* knock-out mice with macrocephaly (Orosco *et al.*, 2014). Our results seem to contrast the *WDFY3*-dependent autophagic attenuation of Wnt signalling through removal of DVL3 aggregates (Gao and Chen, 2010; Kadir *et al.*, 2016). Dvl turnover is accelerated by autophagy under stress conditions (Gao and Chen, 2010), but Dvl degradation takes place through the proteasome pathway (Angers *et al.*, 2006; Chan *et al.*, 2006; Madrzak *et al.*, 2015) even in cells in which autophagy is impaired (Gao and Chen, 2010). We observed no differences in DVL2 or DVL3 in our proteomic analysis of brain cortices, thus the haploinsufficiency in *Wdfy3* and impaired autophagy (Napoli *et al.*, 2018) could be compensated by the upregulation of ubiquitination and proteasome-dependent degradation of Dvl, thereby attenuating Wnt pathway. In accordance with this we see a down-regulation of DVL1 in our proteomics data (Supplementary Table 1) and canonical Wnt signalling was shown to be sensitive to changes in the abundance of either DVL3 or DVL1.

In regard to human macro- and microcephaly, molecular modelling of variant p.(Arg2823Trp) found in one of our macrocephalic probands together with the known microcephaly-associated variant p.(Arg2637Trp) (Kadir *et al.*, 2016) revealed that each variant might cause a destabilization of different *WDFY3* domains, namely the BEACH (Fig. 2B) and the PH-domain respectively (Fig. 2C). Thus, destabilization of different domains may lead to distinct effects on the canonical Wnt pathway and opposite phenotypes with respect to brain size resulting from predicted loss or gain of protein function. In support of this we report on an additional proband with a *de novo* missense-variant also located in the PH-domain, who also presented with intellectual disability and microcephaly (Proband 3; Fig. 1 and Table 1). The function of the PH-domain is unknown, but the close interaction of PH and BEACH domains may lead to functional autoinhibition. Namely, an operative PH-domain would constitutively inhibit the function of the BEACH-domain. While this hypothesis remains purely speculative, we propose a model in which variants that disrupt the PH domain would result in a loss of the auto-inhibition and a consequent gain of function. This would have an opposite effect to truncating variants and variants that are located in the BEACH-domain, which would lead to loss of function.

Further we show that basic parameters of mouse *Wdfy3* neocortical expression during embryonic development are preserved in humans. In human, during the second



trimester, *WDFY3* is highly expressed in pallium; however, not only in a subset of dividing radial glial cells of the ventricular zone as in the mouse, but throughout all layers with ventricular zone and cortical plate showing strongest expression (Fig. 3A–C). This likely points at additional roles that *WDFY3* may exert during human neocortical histogenesis, which requires its continued activity in post-mitotic cells. We noted that in the cortical plate *WDFY3* is retained in distinct radially aligned columns that likely present radial clones originating from the same proliferative units and precursors to the later minicolumnar organization of the neocortex (Fig. 3C). *WDFY3* loss of function may thus promote minicolumn disorganization. Minicolumn structure has been implicated in ASD pathogenesis (McKavanagh *et al.*, 2015) and cognitive performance (Opris and Casanova, 2014).

Additional support for an association between *WDFY3* and cognitive performance comes from the knockdown of the *Drosophila WDFY3* orthologue *Bchs*. *Bchs*-deficient flies show defects in habituation, reflecting alterations in non-associative learning and memory (Stessman *et al.*, 2017). Indeed, the majority of our probands show mild to moderate intellectual disability, sometimes accompanied by behavioural concerns including attention deficit hyperactivity disorder and autism spectrum disorder. In addition, 7 of 13 cases (54%) showed gross motor development delay or muscular hypotonia. This appears to be paralleled by the deficits we observed in associative learning and motor coordination in haploinsufficient mice (Fig. 4).

Based on the concordant human and murine phenotype-genotype correlation and the direct role of *WDFY3* in neuronal development, we conclude that *WDFY3* haploinsufficiency causes mild-to-moderate neurodevelopmental delay, intellectual disability, macrocephaly, and behavioural disorders. *WDFY3* variants produce different phenotypic outcomes with respect to brain size depending on how Wnt pathway is regulated. While, as previously demonstrated, PH domain mutations cause microcephaly, variants putatively resulting in haploinsufficiency lead to macrocephaly.

## Web resources

ClinVar, <https://www.ncbi.nlm.nih.gov/clinvar/>  
 GenBank, <https://www.ncbi.nlm.nih.gov/genbank/>  
 Genome Aggregation Database (gnomAD), <http://gnomad.broadinstitute.org/>  
 HGMD, <http://www.hgmd.cf.ac.uk/ac/index.php>  
 MutationTaster, <http://www.mutationtaster.org/>  
 OMIM, <http://omim.org/>  
 PolyPhen-2, <http://genetics.bwh.harvard.edu/pph2/>  
 Protter, <http://wlab.ethz.ch/protter/>  
 PubMed, <https://www.ncbi.nlm.nih.gov/pubmed/>  
 REVEL: Rare Exome Variant Ensemble Learner, <https://sites.google.com/site/revelgenomics/>  
 RSCB Protein Data Bank, <https://www.rcsb.org/pdb/home/home.do>

UCSC Genome Browser, <https://genome.ucsc.edu/>  
 Varvis, <https://www.limbus-medtec.com/>  
 wANNOVAR, <http://wannovar.wglab.org/>

## Acknowledgements

The authors are thankful to Dr Jimenez-Amaya (Universidad Autónoma de Madrid, Spain) for providing the human embryo brains. We also wish to acknowledge the resources of MSSNG ([www.mssng.org](http://www.mssng.org)), Autism Speaks and The Centre for Applied Genomics at The Hospital for Sick Children, Toronto, Canada. We thank the participants in the Autism Speaks MSSNG program and all families for their time and contributions.

## Funding

D.L.D. is funded through “Clinician Scientist Programm, Medizinische Fakultät der Universität Leipzig”. This study was in part funded by Shriners Hospitals for Children, NICHD R21HD67855 and NIMH R21MH115347 to K.S.Z., the Simons Foundation with SFARI 286567 to K.S.Z., and the Nancy Lurie Marks Family Foundation to K.S.Z., as well as a Shriners Hospitals for Children Postdoctoral Fellowship Grant to L.A.O. Additional support was provided by NICHD U54 HD079125 to J.L.S., M.C.P., J.N.C. NHGRI UM1HG007301 applies to S.M.H and G.M.C. The MIND Institute IDDR is funded by the National Institute of Child Health and Human Development (U54 HD079125).

## Competing interests

All authors declare no conflict of interest. Authors affiliated to GeneDx<sup>10</sup> are employees of GeneDx, Inc., a wholly owned subsidiary of OPKO Health, Inc. S.W.S. holds the GlaxoSmithKline-CIHR Endowed Chair in Genome Sciences at the Hospital for Sick Children and University of Toronto.

## Supplementary material

Supplementary material is available at *Brain* online.

## References

- Adzhubei IA, Schmidt S, Peshkin L, Ramensky VE, Gerasimova A, Bork P, *et al.* A method and server for predicting damaging missense mutations. *Nat Methods* 2010; 7: 248–9.
- Angers S, Thorpe CJ, Biechele TL, Goldenberg SJ, Zheng N, MacCoss MJ, *et al.* The KLHL12-Cullin-3 ubiquitin ligase negatively regulates the Wnt-beta-catenin pathway by targeting Dishevelled for degradation. *Nat Cell Biol* 2006; 8: 348–57.



- Bowling KM, Thompson ML, Amaral MD, Finnila CR, Hiatt SM, Engel KL, et al. Genomic diagnosis for children with intellectual disability and/or developmental delay. *Genome Med* 2017; 9: 43.
- Chan DW, Chan CY, Yam JW, Ching YP, Ng IO. Prickle-1 negatively regulates Wnt/beta-catenin pathway by promoting Dishevelled ubiquitination/degradation in liver cancer. *Gastroenterology* 2006; 131: 1218–27.
- Core Team R. R: a language and environment for statistical computing. Vienna: R Foundation for Statistical Computing; 2017.
- Cullinane AR, Schaffer AA, Huizing M. The BEACH is hot: a LYST of emerging roles for BEACH-domain containing proteins in human disease. *Traffic* 2013; 14: 749–66.
- Fanselow MS. Contextual fear, gestalt memories, and the hippocampus. *Behav Brain Res* 2000; 110: 73–81.
- Filimonenko M, Isakson P, Finley KD, Anderson M, Jeong H, Melia TJ, et al. The selective macroautophagic degradation of aggregated proteins requires the PI3P-binding protein Alfy. *Mol Cell* 2010; 38: 265–79.
- Gao C, Chen YG. Dishevelled: The hub of Wnt signaling. *Cell Signal* 2010; 22: 717–27.
- Gebauer D, Li J, Jogl G, Shen Y, Myszka DG, Tong L. Crystal structure of the PH-BEACH domains of human LRBA/BGL. *Biochemistry* 2004; 43: 14873–80.
- Genomes Project C, Auton A, Brooks LD, Durbin RM, Garrison EP, Kang HM, et al. A global reference for human genetic variation. *Nature* 2015; 526: 68–74.
- Guex N, Peitsch MC. SWISS-MODEL and the Swiss-PdbViewer: an environment for comparative protein modeling. *Electrophoresis* 1997; 18: 2714–23.
- Hormozdiari F, Penn O, Borenstein E, Eichler EE. The discovery of integrated gene networks for autism and related disorders. *Genome Res* 2015; 25: 142–54.
- Iossifov I, O’Roak BJ, Sanders SJ, Ronemus M, Krumm N, Levy D, et al. The contribution of de novo coding mutations to autism spectrum disorder. *Nature* 2014; 515: 216–21.
- Iossifov I, Ronemus M, Levy D, Wang Z, Hakker I, Rosenbaum J, et al. De novo gene disruptions in children on the autistic spectrum. *Neuron* 2012; 74: 285–99.
- Kadir R, Harel T, Markov B, Perez Y, Bakhrat A, Cohen I, et al. ALFY-controlled DVL3 autophagy regulates Wnt signaling, determining human brain size. *PLoS Genet* 2016; 12: e1005919.
- Keller A, Nesvizhskii AI, Kolker E, Aebersold R. Empirical statistical model to estimate the accuracy of peptide identifications made by MS/MS and database search. *Anal Chem* 2002; 74: 5383–92.
- Krumm N, O’Roak BJ, Shendure J, Eichler EE. A de novo convergence of autism genetics and molecular neuroscience. *Trends Neurosci* 2014; 37: 95–105.
- Kumar P, Henikoff S, Ng PC. Predicting the effects of coding non-synonymous variants on protein function using the SIFT algorithm. *Nat Protoc* 2009; 4: 1073–81.
- Kwan V, Unda BK, Singh KK. Wnt signaling networks in autism spectrum disorder and intellectual disability. *J Neurodev Disord* 2016; 8: 45.
- LeDoux J. The emotional brain, fear, and the amygdala. *Cell Mol Neurobiol* 2003; 23: 727–38.
- Lek M, Karczewski KJ, Minikel EV, Samocha KE, Banks E, Fennell T, et al. Analysis of protein-coding genetic variation in 60,706 humans. *Nature* 2016; 536: 285–91.
- Madzrak J, Fiedler M, Johnson CM, Ewan R, Knebel A, Bienz M, et al. Ubiquitination of the Dishevelled DIX domain blocks its head-to-tail polymerization. *Nat Commun* 2015; 6: 6718.
- Martin S, Chamberlin A, Shinde DN, Hempel M, Strom TM, Schreiber A, et al. De Novo variants in GRIA4 lead to intellectual disability with or without seizures and gait abnormalities. *Am J Hum Genet* 2017; 101: 1013–20.
- McDonald L, Rennie A, Tolmie J, Galloway P, McWilliam R. Investigation of global developmental delay. *Arch Dis Child* 2006; 91: 701–5.
- McKavanagh R, Buckley E, Chance SA. Wider minicolumns in autism: a neural basis for altered processing? *Brain* 2015; 138: 2034–45.
- Napoli E, Song G, Panoutsopoulos A, Riyadh M, Kaushik G, Halmaj J, et al. Beyond autophagy: novel role for the autism-linked Wdfy3 gene in brain mitophagy. *Sci Rep* 2018; 8: 11348.
- Nesvizhskii AI, Keller A, Kolker E, Aebersold R. A statistical model for identifying proteins by tandem mass spectrometry. *Anal Chem* 2003; 75: 4646–58.
- Okerlund ND, Cheyette BN. Synaptic Wnt signaling—a contributor to major psychiatric disorders? *J Neurodev Disord* 2011; 3: 162–74.
- Opris I, Casanova MF. Prefrontal cortical minicolumn: from executive control to disrupted cognitive processing. *Brain* 2014; 137: 1863–75.
- Orosco LA, Ross AP, Cates SL, Scott SE, Wu D, Sohn J, et al. Loss of Wdfy3 in mice alters cerebral cortical neurogenesis reflecting aspects of the autism pathology. *Nat Commun* 2014; 5: 4692.
- Petrovski S, Wang Q, Heinzen EL, Allen AS, Goldstein DB. Genic intolerance to functional variation and the interpretation of personal genomes. *PLoS Genet* 2013; 9: e1003709.
- Pollard KS, Hubisz MJ, Rosenbloom KR, Siepel A. Detection of non-neutral substitution rates on mammalian phylogenies. *Genome Res* 2010; 20: 110–21.
- Pruitt KD, Harrow J, Harte RA, Wallin C, Diekhans M, Maglott DR, et al. The consensus coding sequence (CCDS) project: Identifying a common protein-coding gene set for the human and mouse genomes. *Genome Res* 2009; 19: 1316–23.
- Rentzsch P, Witten D, Cooper GM, Shendure J, Kircher M. CADD: predicting the deleteriousness of variants throughout the human genome. *Nucleic Acids Res* 2019; 47: D886–94.
- Retterer K, Juusola J, Cho MT, Vitazka P, Millan F, Gibellini F, et al. Clinical application of whole-exome sequencing across clinical indications. *Genet Med* 2016; 18: 696–704.
- Samocha KE, Robinson EB, Sanders SJ, Stevens C, Sabo A, McGrath LM, et al. A framework for the interpretation of de novo mutation in human disease. *Nat Genet* 2014; 46: 944–50.
- Sayle RA, Milner-White EJ. RASMOL: biomolecular graphics for all. *Trends Biochem Sci* 1995; 20: 374.
- Schwarz JM, Cooper DN, Schuelke M, Seelow D. MutationTaster2: mutation prediction for the deep-sequencing age. *Nat Methods* 2014; 11: 361–2.
- Simonsen A, Birkeland HC, Gillooly DJ, Mizushima N, Kuma A, Yoshimori T, et al. Alfy, a novel FYVE-domain-containing protein associated with protein granules and autophagic membranes. *J Cell Sci* 2004; 117: 4239–51.
- Sobreira N, Schiettecatte F, Valle D, Hamosh A. GeneMatcher: a matching tool for connecting investigators with an interest in the same gene. *Hum Mutat* 2015; 36: 928–30.
- Stessman HA, Xiong B, Coe BP, Wang T, Hoekzema K, Fencikova M, et al. Targeted sequencing identifies 91 neurodevelopmental-disorder risk genes with autism and developmental-disability biases. *Nat Genet* 2017; 49: 515–26.
- Tacchelly-Benites O, Wang Z, Yang E, Lee E, Ahmed Y. Toggling a conformational switch in Wnt/beta-catenin signaling: regulation of axin phosphorylation: the phosphorylation state of axin controls its scaffold function in two Wnt pathway protein complexes. *Bioessays* 2013; 35: 1063–70.
- Tarailo-Graovac M, Zhu JYA, Matthews A, van Karnebeek CDM, Wasserman WW. Assessment of the ExAC data set for the presence of individuals with pathogenic genotypes implicated in severe Mendelian pediatric disorders. *Genet Med* 2017; 19: 1300–8.
- Vissers LE, Gilissen C, Veltman JA. Genetic studies in intellectual disability and related disorders. *Nat Rev Genet* 2016; 17: 9–18.
- Wang T, Guo H, Xiong B, Stessman HA, Wu H, Coe BP, et al. De novo genic mutations among a Chinese autism spectrum disorder cohort. *Nat Commun* 2016; 7: 13316.
- Webb B, Sali A. Protein structure modeling with MODELLER. *Methods Mol Biol (Clifton, NJ)* 2017; 1654: 39–54.

Yuen RK, Merico D, Bookman M, LH J, Thiruvahindrapuram B, Patel RV, et al. Whole genome sequencing resource identifies 18 new candidate genes for autism spectrum disorder. *Nat Neurosci* 2017; 20: 602–11.

Zimmermann L, Stephens A, Nam SZ, Rau D, Kubler J, Lozajic M, et al. A completely reimplemented MPI bioinformatics toolkit with a new HHpred server at its core. *J Mol Biol* 2018; 430: 2237–43.